

JOURNAL ARTICLE

Implicit Sub-stepping Scheme for Critical State Soil Models

Hoang-Giang Bui¹ | Jelena Ninić¹ | Günther Meschke²¹University of Birmingham, School of Engineering, Birmingham, UK²Ruhr University Bochum, Institute for Structural Mechanics, Bochum, Germany**Correspondence**

Hoang Giang Bui, University of Birmingham, UK. Email: b.hoanggiang@bham.ac.uk

Abstract

The stress integration of critical soil model is usually based on implicit Euler algorithm, where the stress predictor is corrected by employing a return mapping algorithm. In the case of large load step, the solution of local nonlinear system to compute the plastic multiplier may not be attained. To overcome this problem, a sub-stepping scheme shall be used to improve the convergence of the local nonlinear system solution strategy. Nevertheless, the complexity of the tangent operator of the sub-stepping scheme is high. This complicates the use of Newton-Raphson algorithm to obtain global quadratic convergence. In this paper, a formulation for consistent tangent operator is developed for implicit sub-stepping integration for the modified Cam-Clay model and unified Clay and Sand model. This formulation is highly efficient and can be used with problem involving large load step, such as tunnel simulation.

KEYWORDS:

Modified Cam-Clay, CASM, sub-stepping scheme, implicit integration

1 | INTRODUCTION

The introduction of critical soil models marks an important advance in computational geomechanics. Based on elastoplastic theory, the model is first proposed by Roscoe and coworkers^{1,2} as Cam-Clay model (CC), and subsequently improved as modified Cam-Clay model³. The modified Cam-Clay model (MCC) is shown to sufficiently predict main attributes of the constitutive behavior of normally consolidated soft cohesive soils⁴, although deficiencies were reported when modeling highly overconsolidated soils. Later, Yu⁵ generalized the standard Cam-Clay model to allow modeling the behavior of sand. The unified model, denoted as CASM^{5,6}, has the ability to resolve some drawbacks of the standard Cam-Clay models, such as the overestimation of the strength on the “dry side” or the behavior of loose sand in undrained tests, while limiting the number of parameters to seven, which is an advantage to adopt the model both in academic research and practical applications.

To apply the critical soil models in numerical simulations, an integration algorithm is required. In the context of implicit methods, the backward Euler algorithm is typically used. This is frequently resorted to the return mapping algorithm^{7,8}, which will ensure quadratic convergence of the Newton-Raphson algorithm if certain conditions are satisfied. The advantage of the implicit method is its robustness, second-order accuracy and able to use with large load step. Nevertheless, the implicit algorithm typically requires the high-order derivatives of yield functions and plastic flow rule. The return mapping algorithm has been successfully applied to Cam-Clay models in⁹ and, being extended to the finite strain regime, in¹⁰. Further applications of the return map algorithm to extensions of the Cam Clay model have been suggested in^{11,12,13}.

In contrast to implicit methods, explicit methods, based on the forward Euler integration, requires only the first order approximation of the yield surface and plastic flow rule and it is considered to be more straightforward to implement. Because only first order accuracy is attained, the load step must be sufficiently small to reduce the accumulated error. The efficiency and robustness of explicit algorithms has been substantially improved by using sub-stepping algorithms^{14,15,16,17}. An automatic error control for sub-stepping algorithm is proposed in¹⁸.

It is well known from analysis of convergence properties of stability of the Newton algorithm, from applications reported in the literature^{19?}, and also experienced by the authors, that the computational robustness of implicit integration schemes applied to elastoplastic models, and, in particular, to critical state models, is limited, and that no convergence of the local iterative scheme at the integration point level is attained when the load step is large. Therefore, it is crucial to sub-divide the load into smaller increments to ensure the existence of local admissible stress state and the convergence of the local iteration, to compute the internal variables and the plastic increment. Because the sub-load increment can be adjusted, this scheme is highly effective for problems, in which the loading path is difficult to control. An example of this class of problems are excavation problems, which are a priori stress control problems if no arc length methods are applied. A consistent sub-stepping scheme has been proposed for elastoplastic models in²⁰. In this paper the trial stress predictor uses a linear extrapolation based on a (constant) elastic tangent, which is typically used for elastoplastic material models. However, this scheme is not optimal for critical state soil models, because the stress-strain rule in the elastic region of the critical state model is nonlinear³.

In Section 2 of this paper, a sub-stepping algorithm for the implicit integration algorithm for critical state soil models, more specifically for the Modified Cam Clay model and the Clay and Sand model, is proposed, which makes use of the more accurate nonlinear approximation of hydrostatic pressure. The effectiveness of the implicit sub-stepping scheme is demonstrated by selected numerical examples presented in Section 3. The findings from these analyses are concluded in Section 4.

2 | IMPLICIT INTEGRATION OF THE CRITICAL STATE SOIL MODELS

In this section, the basic governing equations of the Modified Cam-Clay (MCC) (Section 2.1) model and the Clay and Soil model (Section 2.2) are summarized before an implicit integration algorithm incorporating sub-stepping is elaborated for both models in subsections Section 2.4.

2.1 | Brief summary of the modified Cam-Clay model

The Modified Cam-Clay (MCC) model^{2,21} is characterized by a yield surface formulated in the $p - q$ plane by:

$$f^{\text{MCC}}(p, q, p_c) = \left(\frac{q}{M} \right)^2 + p(p - p_c), \quad (1)$$

by the associative plastic potential $g^{\text{MCC}}(p, q, p_c) = f^{\text{MCC}}(p, q, p_c)$ and by the nonlinear stress-strain relation in the elastic domain:

$$\dot{p} = K \dot{\epsilon}_v^e, \quad \dot{\mathbf{s}} = 2\mu \dot{\epsilon}_d^e. \quad (2)$$

The shear modulus and the pressure-dependent compression modulus K are given as

$$K = \frac{1+e}{\kappa} p, \quad \mu = Kr, \quad r = \frac{3}{2} \frac{1-2\nu}{1+\nu}, \quad (3)$$

and the hardening rule is specified as

$$\dot{p}_c = \theta p_c \dot{\epsilon}_v^p, \quad \theta = \frac{1+e}{\lambda - \kappa}. \quad (4)$$

In Equations (1) to (4), $M, e, \lambda, \kappa, \nu$ are material constants and have following meanings: M is the slope of the critical state line, e is the void ratio, λ is the compression index, κ is the swelling index and ν is the Poisson ratio. For the details on the material parameters and their roles in reflecting the characteristics of soil, the reader is referred to²². p denotes the hydrostatic pressure and q is the deviatoric invariant $q = \sqrt{3/2 \mathbf{s} : \mathbf{s}}$, with $\mathbf{s} = \boldsymbol{\sigma} - p\mathbf{I}$ as the deviatoric stress and $p = \frac{1}{3} \text{tr}(\boldsymbol{\sigma})$. The subscript $(\bullet)_v$ denotes the volumetric component and $(\bullet)_d$ denotes the deviatoric component of the strain. The superscript $(\bullet)^e$ denotes the elastic component and $(\bullet)^p$ denotes the plastic component of the strain. The void ratio e is considered not to change significantly during a load step and is kept fixed within one increment.

2.2 | Brief summary of the CASM model

The Clay and Sand model (CASM) model, as proposed in⁵, adopts the yield surface:

$$f^{\text{CASM}}(p, q, p_c) = \left(\frac{q}{Mp} \right)^N + \frac{1}{\ln R} \ln \frac{p}{p_c}, \quad (5)$$

and the non-associative plastic potential:

$$g^{\text{CASM}}(p, q) = 3M \ln \frac{p}{\beta} + (3 + 2M) \ln \left(2\frac{q}{p} + 3 \right) - (3 - M) \ln \left(3 - \frac{q}{p} \right). \quad (6)$$

β is a size parameter and dependent on the stress state. It can be obtained by solving $g^{\text{CASM}}(p, q) = 0$ at a plastic state. The stress-strain relation in the elastic domain and the hardening rule (4) are similar to the MCC model (see (2) and (3)). In addition to the material parameters $M, e, \lambda, \kappa, \mu$, the CASM model is characterized by additional parameters N and R defining the shape of the yield surface in the deviatoric plane. N is the parameter controlling the shape of the yield surface and R is the spacing ratio. The CASM model can be adjusted to reproduce the standard Cam-Clay model. For example, the original CC model can be obtained by setting $N = 1$ and $\ln R = 1$, while the MCC model can be approximated by setting $R = 2$ and a suitable value for N . For more details on the theoretical basis of CASM model, the reader is referred to⁵.

2.3 | One-step implicit integration scheme

In the one-step integration scheme, the hydrostatic pressure is approximated by integrating the rate form of nonlinear stress-strain relation (see Equation (2))²³. It is summarized here to serve as the basis for sub-stepping scheme proposed in the next Subsection.

2.3.1 | Stress integration algorithm

We denote $\{p_{n+1}, q_{n+1}, (p_c)_{n+1}\}$ as the state variables at the current load step and $\Delta\epsilon = \epsilon_{n+1} - \epsilon_n$ as the incremental total strain obtained from the solution of the equilibrium equations on the structural level for load step $n + 1$. For brevity, the step index $n + 1$ of the current step is neglected in what follows. In the predictor step, which assumes pure elastic loading ($\Delta\epsilon_v^e = \Delta\epsilon_v$), the stresses and shear stiffness are calculated as:

$$p = p_n \exp\left(\frac{1+e}{\kappa} \Delta\epsilon_v\right), \quad \mathbf{s} = \mathbf{s}_n + 2\bar{\mu} \Delta\epsilon_d, \quad p_c = (p_c)_n, \quad \bar{\mu} = \frac{p - p_n}{\Delta\epsilon_v} r. \quad (7)$$

If the yield condition in the predictor step is violated ($f(p, q, p_c) > 0$), the material point is subjected to plastic loading, and $\{p, q, p_c\}$ along with the increment of the plastic multiplier $\Delta\phi$ need to be determined from the solution of the following set of nonlinear equations, which holds for any Critical State model:

$$h_1 = p - p_n \exp\left(\frac{1+e}{\kappa} \Delta\epsilon_v^e\right) = 0, \quad (8)$$

$$h_2 = q - \sqrt{\frac{3}{2}} \|\mathbf{s}_n + 2\bar{\mu} \Delta\epsilon_d^e\| = 0, \quad \bar{\mu} = \frac{p - p_n}{\Delta\epsilon_v^e} r, \quad (9)$$

$$h_3 = p_c - (p_c)_n \exp(\theta \Delta\epsilon_v^p) = 0, \quad (10)$$

$$h_4 = f(p, q, p_c) = 0. \quad (11)$$

The solution for the set of unknowns $\{p, q, p_c, \Delta\phi\}$ of the nonlinear system eqs. (8) to (11) can be determined by using the implicit Newton-Raphson algorithm. For details of the linearization of the residuals from the nonlinear system when using the Newton-Raphson method for the MCC model, the reader is referred to²³. For the CASM model, the reader is referred to Appendix C.

2.3.2 | Consistent tangent operator

With the solution for the stress state and the hardening variables at hand, the consistent tangent operator can be defined as:

$$\mathbb{C} = \frac{\partial \boldsymbol{\sigma}}{\partial \Delta \boldsymbol{\varepsilon}} = \frac{\partial \mathbf{s}}{\partial \Delta \boldsymbol{\varepsilon}} + \mathbf{I} \otimes \frac{\partial p}{\partial \Delta \boldsymbol{\varepsilon}}. \quad (12)$$

The consistent tangent operator \mathbb{C} is crucial to preserve the quadratic rate of convergence of the fully implicit Newton-Raphson strategy. In the elastic state, the components $\frac{\partial \mathbf{s}}{\partial \Delta \boldsymbol{\varepsilon}}$ and $\frac{\partial p}{\partial \Delta \boldsymbol{\varepsilon}}$ of (12) can be straightforwardly calculated by taking the linearization of (7):

$$\frac{\partial p}{\partial \Delta \boldsymbol{\varepsilon}} = K \mathbf{I}, \quad \frac{\partial \mathbf{s}}{\partial \Delta \boldsymbol{\varepsilon}} = 2\bar{\mu} \mathbb{1}_d + 2\Delta \boldsymbol{\varepsilon}_d \otimes \frac{\partial \bar{\mu}}{\partial \Delta \boldsymbol{\varepsilon}}, \quad \frac{\partial \bar{\mu}}{\partial \Delta \boldsymbol{\varepsilon}} = \frac{Kr - \bar{\mu}}{\Delta \varepsilon_v} \mathbf{I}, \quad K = \frac{1+e}{\kappa} p. \quad (13)$$

In the case that the strain increment in the integration point is leading to an elasto-plastic response in the current increment, $\frac{\partial p}{\partial \Delta \boldsymbol{\varepsilon}}$, $\frac{\partial p_c}{\partial \Delta \boldsymbol{\varepsilon}}$ and $\frac{\partial \mathbf{s}}{\partial \Delta \boldsymbol{\varepsilon}}$ can be written in terms of $\frac{\partial \Delta \phi}{\partial \Delta \boldsymbol{\varepsilon}}$ as:

$$\frac{\partial p}{\partial \Delta \boldsymbol{\varepsilon}} = \mathbf{A} + a \frac{\partial \Delta \phi}{\partial \Delta \boldsymbol{\varepsilon}}, \quad \frac{\partial p_c}{\partial \Delta \boldsymbol{\varepsilon}} = \mathbf{B} + b \frac{\partial \Delta \phi}{\partial \Delta \boldsymbol{\varepsilon}}, \quad \frac{\partial \mathbf{s}}{\partial \Delta \boldsymbol{\varepsilon}} = \mathbb{D} + \mathbf{D} \otimes \frac{\partial \Delta \phi}{\partial \Delta \boldsymbol{\varepsilon}}. \quad (14)$$

In analogy, linearization of q is obtained as:

$$\frac{\partial q}{\partial \Delta \boldsymbol{\varepsilon}} = \frac{3}{2} \frac{1}{q} \left(\mathbf{s} : \frac{\partial \mathbf{s}}{\partial \Delta \boldsymbol{\varepsilon}} \right) = \frac{3}{2} \frac{1}{q} \left(\mathbf{s} : \mathbb{D} + (\mathbf{s} : \mathbf{D}) \frac{\partial \Delta \phi}{\partial \Delta \boldsymbol{\varepsilon}} \right). \quad (15)$$

For the MCC model, linearization of the yield function (1) leads to:

$$\frac{2q}{M^2} \frac{\partial q}{\partial \Delta \boldsymbol{\varepsilon}} + \frac{\partial p}{\partial \Delta \boldsymbol{\varepsilon}} (p - p_c) + p \left(\frac{\partial p}{\partial \Delta \boldsymbol{\varepsilon}} - \frac{\partial p_c}{\partial \Delta \boldsymbol{\varepsilon}} \right) = 0. \quad (16)$$

Eq. 16 allows to incorporate (14) and (15) to (16), which then effectively leads to an equation to determine $\frac{\partial \Delta \phi}{\partial \Delta \boldsymbol{\varepsilon}}$ for the MCC model:

$$\left[\frac{3}{M^2} \mathbf{s} : \mathbf{D} + (2p - p_c) a - pb \right] \frac{\partial \Delta \phi}{\partial \Delta \boldsymbol{\varepsilon}} = - (2p - p_c) \mathbf{A} + p \mathbf{B} - \frac{3}{M^2} \mathbf{s} : \mathbb{D}. \quad (17)$$

For the CASM model, linearization of the yield function (5) leads to:

$$\frac{1}{p} \left[\frac{1}{\ln R} - N \left(\frac{q}{Mp} \right)^N \right] \frac{\partial p}{\partial \Delta \boldsymbol{\varepsilon}} + \frac{Nq^{N-1}}{(Mp)^N} \frac{\partial q}{\partial \Delta \boldsymbol{\varepsilon}} - \frac{1}{\ln R} \frac{1}{p_c} \frac{\partial p_c}{\partial \Delta \boldsymbol{\varepsilon}} = 0, \quad (18)$$

Substituting (14) and (15) into (18) leads to an equation to determine $\frac{\partial \Delta \phi}{\partial \Delta \epsilon}$ for the CASM model:

$$\left(\frac{a}{p} \left[\frac{1}{\ln R} - N \left(\frac{q}{Mp} \right)^N \right] + \frac{3}{2} \frac{Nq^{N-2}(\mathbf{s} : \mathbf{D})}{(Mp)^N} - \frac{1}{\ln R} \frac{b}{p_c} \right) \frac{\partial \Delta \phi}{\partial \Delta \epsilon} = -\frac{\mathbf{A}}{p} \left[\frac{1}{\ln R} + N \left(\frac{q}{Mp} \right)^N \right] + \frac{3}{2} \frac{Nq^{N-2}(\mathbf{s} : \mathbb{D})}{(Mp)^N} + \frac{1}{\ln R} \frac{\mathbf{B}}{p_c}. \quad (19)$$

Solving (17) and (19), respectively, the consistent tangent operator for both models can be calculated using (14) and (12). Details of the derivation of the terms \mathbf{A} , a , \mathbf{B} , b , \mathbf{D} and \mathbb{D} , are contained in the Appendix A for the MCC model, and in the Appendix D for the CASM model.

2.4 | Sub-stepping integration scheme

2.4.1 | Stress integration algorithm

In the sub-stepping integration scheme, the strain increment $\Delta \epsilon$ is divided into sub-increments

$$\Delta \epsilon = \sum_{k=1}^m {}^k \Delta \epsilon, \quad {}^k \Delta \epsilon = \alpha_k \Delta \epsilon, \quad \sum_{k=1}^m \alpha_k = 1. \quad (20)$$

where m is the number of sub-steps. The stress integration in one sub-step is the same as in the one-step scheme in Section 2.3, with the initial state of sub-step $k+1$ defined as the state of the previous sub-step k . The stress at the end of the sub-step k is denoted as ${}^k \sigma$. The final stress is the stress obtained in sub-step $k=m$: $\sigma_{n+1} = {}^m \sigma_{n+1}$. Evidently, the one-step algorithm is a particular case of the sub-stepping algorithm, with the number of sub-steps set to one.

2.4.2 | Consistent tangent operator

The tangent operator $\frac{\partial {}^k \sigma}{\partial {}^k \Delta \epsilon}$ can be computed using the approach of one-step scheme. Nevertheless, the tangent operator $\frac{\partial \sigma}{\partial \Delta \epsilon} = \frac{\partial {}^m \sigma}{\partial \Delta \epsilon}$ cannot be trivially computed as the sum of the tangent operators in the individual sub-step, since ${}^{k+1} \sigma$ depends on ${}^k \sigma$ and ${}^{k+1} \Delta \epsilon$. Instead, $\frac{\partial {}^k \sigma}{\partial \Delta \epsilon}$ shall be determined for all sub-steps.

From (12), one obtains $\frac{\partial {}^k \sigma}{\partial \Delta \epsilon} = \frac{\partial {}^k \mathbf{s}}{\partial \Delta \epsilon} + \mathbf{I} \otimes \frac{\partial {}^k p}{\partial \Delta \epsilon} \cdot \frac{\partial {}^k \mathbf{s}}{\partial \Delta \epsilon}$ and $\frac{\partial {}^k p}{\partial \Delta \epsilon}$ can be determined recursively, as presented in the following: Firstly, $\frac{\partial {}^k \mathbf{s}}{\partial {}^k \Delta \epsilon}$, $\frac{\partial {}^k p}{\partial {}^k \Delta \epsilon}$, $\frac{\partial {}^k p_c}{\partial {}^k \Delta \epsilon}$ with $k=1$ can be determined using the one-step scheme in Section 2.3. Applying (20) leads to the consistent linearization of the stresses in sub-step $k=1$: $\frac{\partial {}^1 \mathbf{s}}{\partial \Delta \epsilon} = \alpha_1 \frac{\partial {}^1 \mathbf{s}}{\partial {}^1 \Delta \epsilon}$, $\frac{\partial {}^1 p}{\partial \Delta \epsilon} = \alpha_1 \frac{\partial {}^1 p}{\partial {}^1 \Delta \epsilon}$ and $\frac{\partial {}^1 p_c}{\partial \Delta \epsilon} = \alpha_1 \frac{\partial {}^1 p_c}{\partial {}^1 \Delta \epsilon}$. Secondly, assuming $\frac{\partial {}^k \mathbf{s}}{\partial \Delta \epsilon}$, $\frac{\partial {}^k p}{\partial \Delta \epsilon}$ and $\frac{\partial {}^k p_c}{\partial \Delta \epsilon}$ are already known from the previous sub-step, the linearization in the current sub-step $k+1$ is formulated depending, if the current sub-step is an elastic or an elasto-plastic step:

Elastic state:

If the sub-step $(k+1)$ is elastic, the following relations hold:

$${}^{k+1} p = {}^k p \exp \left(\frac{1 + e^{k+1} \Delta \epsilon_v}{\kappa} \right), \quad {}^{k+1} \mathbf{s} = {}^k \mathbf{s} + 2\bar{\mu} {}^{k+1} \Delta \epsilon_d, \quad \bar{\mu} = \frac{{}^{k+1} p - {}^k p}{{}^{k+1} \Delta \epsilon_v} r. \quad (21)$$

Taking the linearization of (21) leads to

$$\frac{\partial^{k+1} p}{\partial \Delta \epsilon} = \frac{k+1}{k} p \frac{\partial^k p}{\partial \Delta \epsilon} + \alpha_{k+1} {}^{k+1} K \mathbf{I}, \quad \frac{\partial^{k+1} \mathbf{s}}{\partial \Delta \epsilon} = \frac{\partial^k \mathbf{s}}{\partial \Delta \epsilon} + 2\alpha_{k+1} \bar{\mu} \mathbb{I}_d + 2 {}^{k+1} \Delta \epsilon_d \otimes \frac{\partial \bar{\mu}}{\partial \Delta \epsilon}, \quad (22)$$

with

$$\frac{\partial \bar{\mu}}{\partial \Delta \epsilon} = \frac{\bar{\mu}}{k} p \frac{\partial^k p}{\partial \Delta \epsilon} + \alpha_{k+1} \frac{{}^{k+1} K r - \bar{\mu}}{{}^{k+1} \Delta \epsilon_v} \mathbf{I}, \quad {}^{k+1} K = \frac{1 + e^{k+1}}{\kappa} p. \quad (23)$$

Elasto-plastic state: The linearizations $\frac{\partial^{k+1} \mathbf{s}}{\partial \Delta \epsilon}$, $\frac{\partial^{k+1} p}{\partial \Delta \epsilon}$ and $\frac{\partial^{k+1} p_c}{\partial \Delta \epsilon}$ in the plastic state are re-written in terms of $\frac{\partial^{k+1} \Delta \phi}{\partial \Delta \epsilon}$. To simplify notation, $\frac{\partial^{k+1} \Delta \phi}{\partial \Delta \epsilon}$ will be denoted as $\frac{\partial \Delta \phi}{\partial \Delta \epsilon}$ for brevity:

$$\frac{\partial^{k+1} p}{\partial \Delta \epsilon} = \mathbf{A} + a \frac{\partial \Delta \phi}{\partial \Delta \epsilon}, \quad \frac{\partial^{k+1} p_c}{\partial \Delta \epsilon} = \mathbf{B} + b \frac{\partial \Delta \phi}{\partial \Delta \epsilon}, \quad \frac{\partial^{k+1} \mathbf{s}}{\partial \Delta \epsilon} = \mathbb{D} + \mathbf{D} \otimes \frac{\Delta \phi}{\Delta \epsilon}. \quad (24)$$

The procedure to compute $\frac{\partial \Delta \phi}{\partial \Delta \epsilon}$ is analogous to the one-step scheme for the elasto-plastic state (see Section 2.3.2). The derivation of the terms \mathbf{A} , a , \mathbf{B} , b , \mathbf{D} and \mathbb{D} for the sub-step $k + 1$ can be found in Appendix B for the MCC model, and Appendix E for the CASM model.

3 | NUMERICAL EXAMPLES

3.1 | Triaxial test of a soil sample

In the first example, the drained compressive triaxial test on a cube sample is performed to validate the accuracy of the implicit sub-stepping algorithm. The geometry and boundary condition can be seen in Figure 1, in which the top surface is applied with prescribed displacement u_v and the sides are applied with prescribed displacement u_h . The geometry is meshed with single hexahedra element with 8 nodes. The test is performed on 3 clay samples with the initial stress state as normally consolidated (case 1, OCR = 1), lightly over-consolidated (case 2, OCR = 2) and highly over-consolidated (case 3, OCR = 5). The proportional loading scheme is selected as the controlled stress path, for which the analytical solution exists. For MCC model, the analytical solution subjected to drained proportional loading can be found in²⁴, and for the CASM model, in Appendix F. In the proportional loading scheme, the load is controlled in such a way that $\dot{q} = k\dot{p}$ (k : loading rate). To produce the stress path that matches with the analytical solution, the axial strain ϵ_a is controlled to match with the displacement history of the analytical solution. It is noted that $\epsilon_a = \frac{1}{3}\epsilon_v + \epsilon_q$, in which ϵ_v is the volumetric strain and ϵ_q is the shear strain.

In the simulation, the following parameters are used for the MCC model: $\{ \lambda = 0.066, \kappa = 0.0077, M = 1.2, e = 1.788, \nu = 0.3 \}$; and for the CASM model: $\{ \lambda = 0.066, \kappa = 0.0077, N = 3, M = 1.2, R = 2.0, e = 1.788, \nu = 0.3 \}$. The implicit sub-stepping algorithm is enforced to run with 2 sub-steps. The loading rate is selected as $k = 3$.

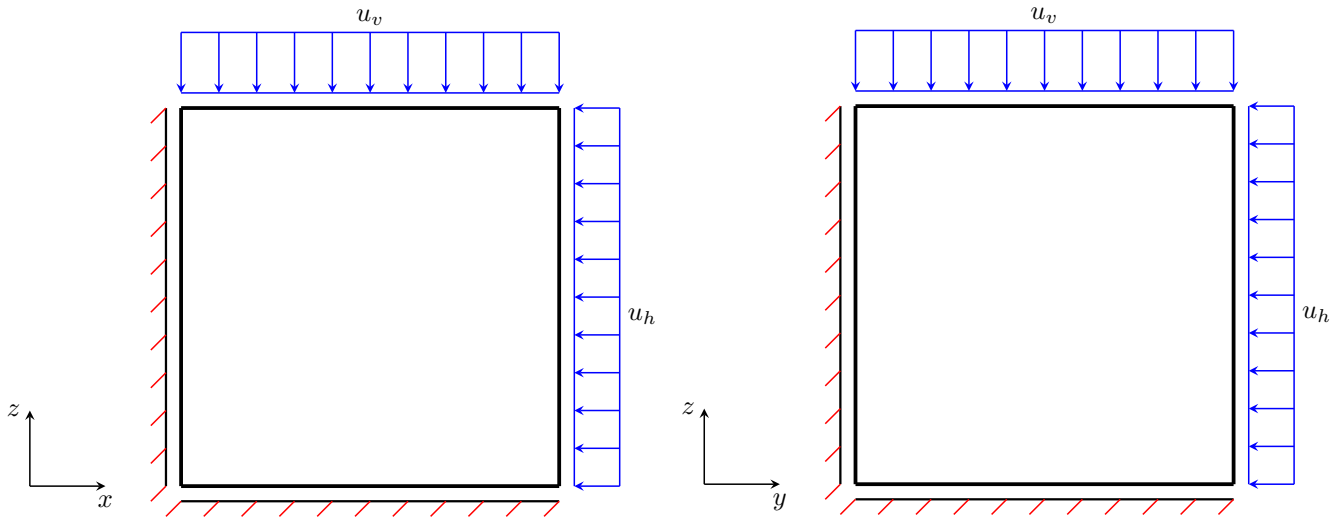


FIGURE 1 Triaxial test example: Illustration of geometry and boundary conditions.

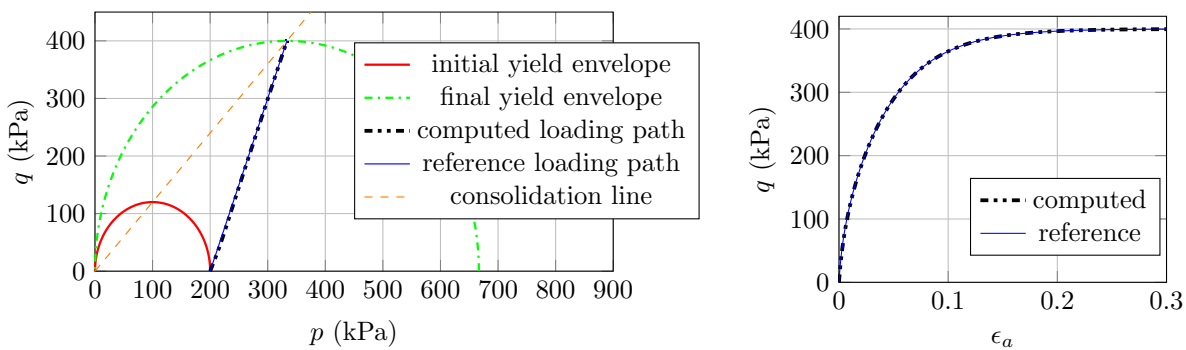


FIGURE 2 Triaxial test example, MCC model, case 1: Left) computed stress path and Right) Load-displacement curve.

3.1.1 | Results with MCC model

The results, as presented in Figure 2 for normally consolidated soil, Figure 3 for lightly consolidated soil and Figure 4 for highly consolidated soil show excellent agreement with the analytical results. In case 1, the stress state starts from the initial yield envelope and stops at the consolidation line as expected. The shear stress asymptotically converges and the soil sample cannot sustain further load. Figure 2 shows the computed stress path (Left) and the according load-displacement curve (Right). The same behaviour is observed for case 2, where the stress state starts from the elastic domain and enters the plastic state after hitting the initial yield envelope (see Figure 3 (Left)). From that point, the soil sample starts to harden and the shear stress asymptotically converges (see Figure 3 (Right)). Case 1 and case 2 show that the implicit sub-stepping algorithm works well on the dry side of the modified Cam-Clay model.

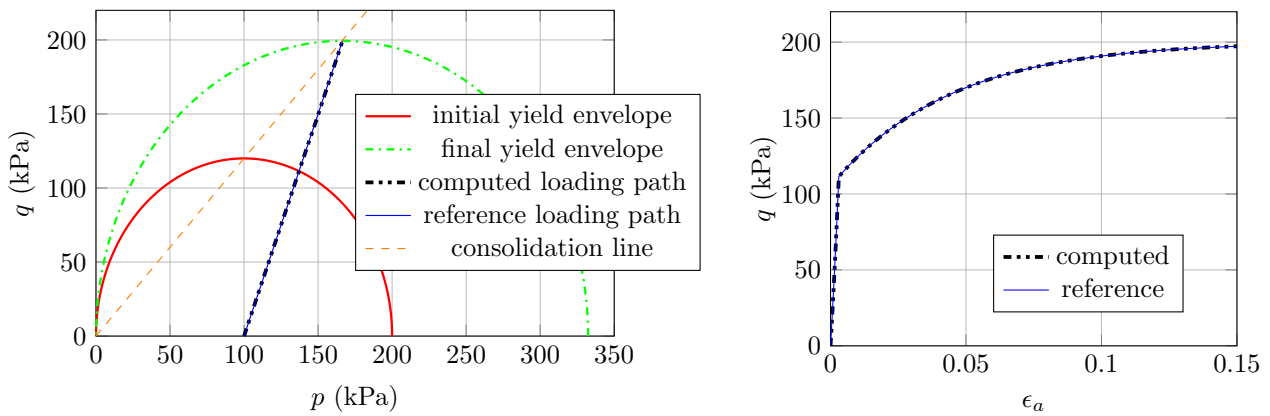


FIGURE 3 Triaxial test example, MCC model, case 2: Left) computed stress path and Right) Load-displacement curve.

In case 3, the softening behaviour on the wet side of the MCC is tested. As can be seen in Figure 4 (Left), the stress state starts in the elastic domain and after hitting the initial yield envelope, it starts to soften and the shear stress asymptotically converges (see Figure 4 (Right)). The stress state ultimately stops at the consolidation line as expected.

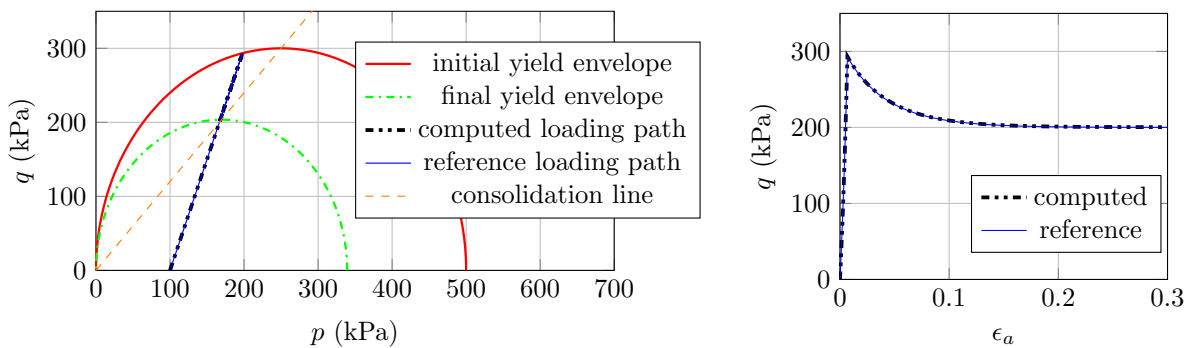


FIGURE 4 Triaxial test example, MCC model, case 3: Left) computed stress path and Right) Load-displacement curve.

3.1.2 | Results with CASM model

The implicit sub-stepping algorithm also work expectedly with the CASM model in the triaxial test, as shown in Figure 5 (case 1), Figure 6 (case 2) and Figure 7 (case 3). For each case, the evolution of the stress state is analogous to the respective case of MCC model. Nevertheless, the stress state hits the initial yield envelope early for case 3 and lately in case 2 due to the shape of the yield surface. Similar to the MCC case, the implicit sub-stepping algorithm also performs well on the wet side of the CASM model.

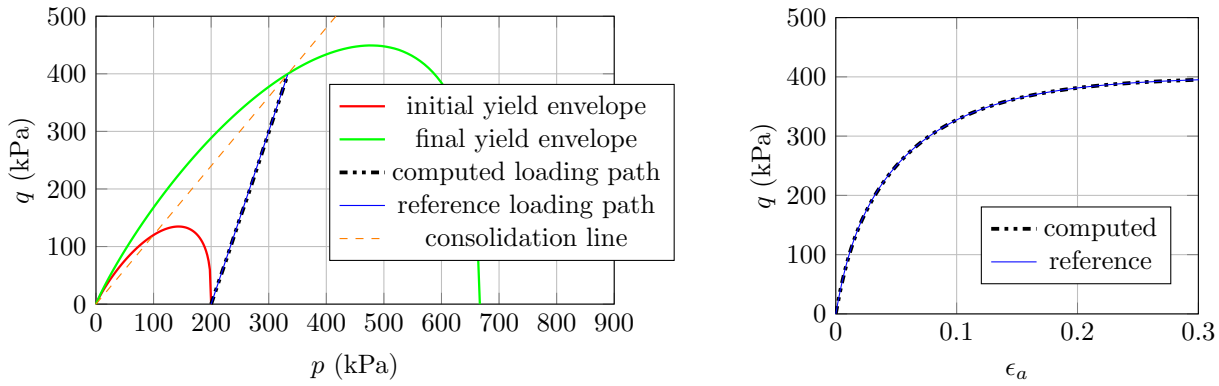


FIGURE 5 Triaxial test example, CASM model, case 1: Left) computed stress path and Right) Load-displacement curve.

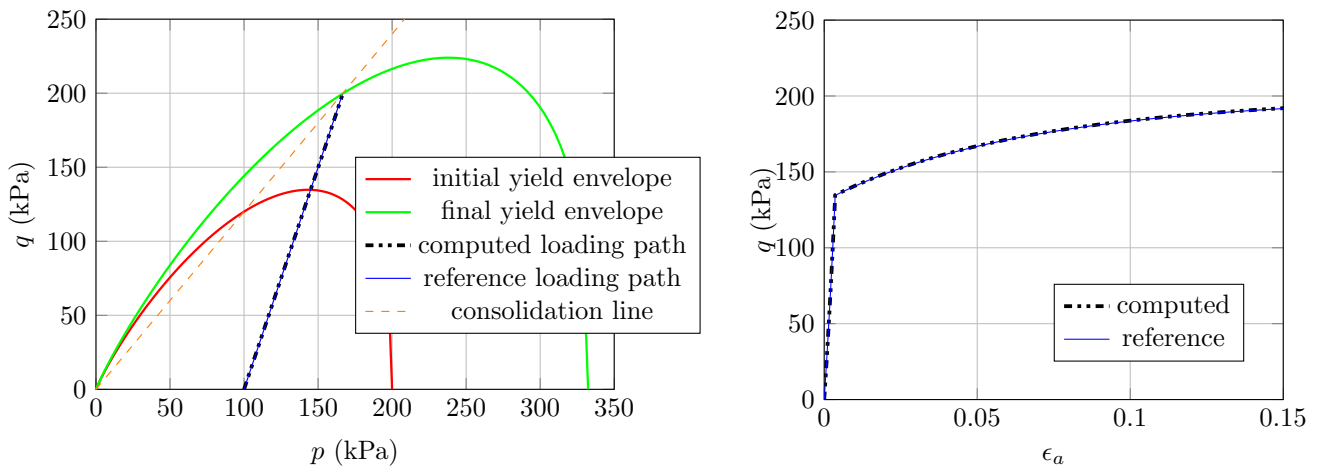


FIGURE 6 Triaxial test example, CASM model, case 2: Left) computed stress path and Right) Load-displacement curve.

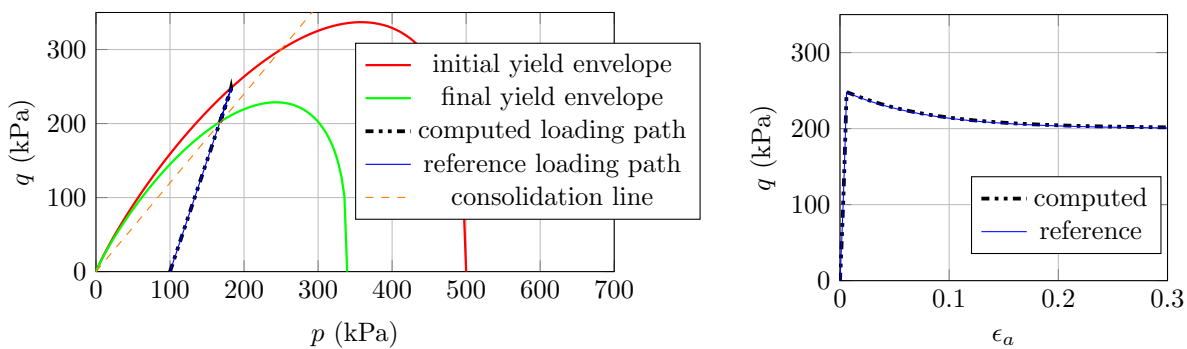


FIGURE 7 Triaxial test example, CASM model, case 3: Left) computed stress path and Right) Load-displacement curve.

3.2 | Excavation of a soil block

In this example, the simulation of the excavation process of a soil block is presented to demonstrate the use of the implicit sub-stepping integration algorithm of MCC and CASM model in a practical application. The geometry and material parameters

for this example are taken from²³. For MCC model, the material parameters read: $\lambda = 0.37$, $\kappa = 0.054$, $M = 1.4$, $e = 2.52$ and $\nu = 0.35$. For CASM model, additional parameters are set, in which $N = 1.4$ and $R = 2.0$, to approximately match the corresponding MCC model. In difference to the original example, the over-consolidation ratio (OCR) is preset to 1.7 for the half upper part and OCR = 1.0 for the half lower part of the soil block. The initial stress of the soil are generated by K_0 -procedure with $K_0 = 1.2$ and the soil density is $\rho = 1732 \text{ kg/m}^3$. The preconsolidation pressure are generated from the initial stress using the yield criteria and OCR as below:

- for MCC:

$$p_c = \text{OCR} \left(p + \frac{q^2}{M^2 p} \right). \quad (25)$$

- for CASM:

$$p_c = \text{OCR} p \exp \left[\ln R \left(\frac{q}{Mp} \right)^N \right]. \quad (26)$$

The sub-stepping algorithm is used by default, and the number of sub-steps are fixed to 4. Using the same analysis sequence as the original example²³, the analysis with different number of steps are simulated. With a total of 8 element layers representing the excavation domain, the number of excavation steps (lifts) are simulated as 8, 4, 2, 1 corresponding to 1, 2, 4, 8 number of excavated layers per excavation step, respectively. The displacements of reference point A²³ corresponding to different lifts, together with the number of average iterations in an excavation step, are reported in Table 1. It is noted that, the displacements are presented in *mm* and the tolerance for convergence is 10^{-13} .

No. of lifts	MCC			CASM		
	d_u	d_v	No. iter/lift	d_u	d_v	No. iter/lift
1	-29.45	-16.76	9	-30.28	-15.53	9
2	-28.67	-16.47	7	-29.58	-15.38	7
4	-28.18	-16.37	6	-29.09	-15.29	6.2
8	-28.02	-16.25	5.5	-28.85	-15.11	5.6

TABLE 1 Excavation of a soil block: Displacements at the reference point A²³ and the convergence of the implicit sub-stepping integration algorithm for different number of lifts.

From Table 1, one can see that the difference in displacements measured at the reference point of MCC and CASM model are not large. This is expected since the yield surface of MCC and CASM are approximately matched. In addition, the convergence of the implicit sub-stepping algorithm exhibits quadratic convergence behaviour, which take a minimum of 5 iteration and maximum 9 iterations to converge in a single load step.

3.3 | Tunnel excavation example

In the third example, a simulation of tunnel excavation employing NATM method is presented. The objective of this example is to illustrate the advantage of implicit sub-stepping algorithm over the one-step algorithm in which the latter one fails to work, which means the implicit sub-stepping algorithm does not converge in one step. The criteria of the local failure is either the non-convergence of the local Newton-Raphson iteration to solve the local nonlinear system, or the inadmissibility of the resulting stress state, i.e. $p \leq 0 \vee q < 0 \vee p_c \leq 0$.

Figure 8 shows the geometry and boundary conditions of the problem at hand. They are adopted from the tutorial 7 of ADONIS geotechnical software²⁵. The following parameters are adopted for the MCC and CASM model: $\lambda = 0.147$, $\kappa = 0.06$, $M = 1.05$, $e = 3.56$ and $\nu = 0.3$. For CASM, additional parameters are used: $N = 1.4$ and $R = 2.0$ to approximate the respective MCC model. The geometry of the problem is meshed by 5231 quadratic quadrilateral element (9-node quad) and the full integration scheme with 9 integration points per element is used.

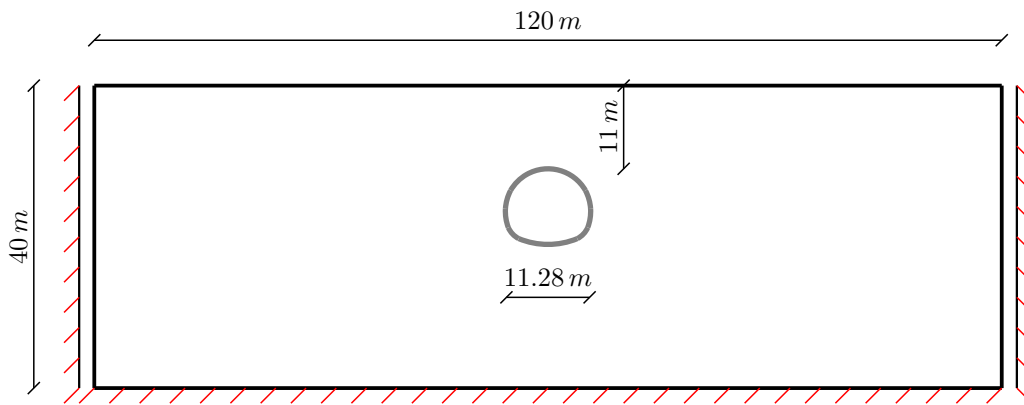


FIGURE 8 Tunnel excavation example: Illustration of geometry and boundary conditions.

Because the number of required sub-steps is not known in advance, an adaptive stepping scheme is used in accordance with the implicit sub-stepping algorithm. If the integration at a sub-step fails, the number of sub-steps at the integration point will be doubled and the sub-stepping integration is started over. Tolerance of 10^{-8} is adopted for the local iteration and tolerance of 10^{-10} is adopted for the global Newton-Raphson loop.

Analogous to the previous example, the initial stress state is generated using K_0 -procedure with $K_0 = 0.5$, $\rho = 1732 \text{ kg/m}^3$ and the initial preconsolidation pressure profile is computed using Equation (25) for MCC and Equation (26) for CASM respectively. The over-consolidation ratio is set to $\text{OCR} = 2.0$.

To simulate the excavation process, a stress relaxation approach is adopted. At first, the elements in the excavation domain are deactivated and the corresponding traction is applied on the tunnel wall to maintain the equilibrium. The traction is computed from the initial stress field within the soil. In the second step, the traction is reduced to 40 %. Subsequently, the shotcrete,

represented by beam elements is installed in the current configuration. The parameters for the shotcrete beam element are $E = 1.56e6 \text{ kPa}$, $\nu = 0.2$ and the thickness is $t = 0.1 \text{ m}$. Finally, after the shotcrete is installed, the applied traction on tunnel wall is removed. The plane strain condition is assumed in the analysis.

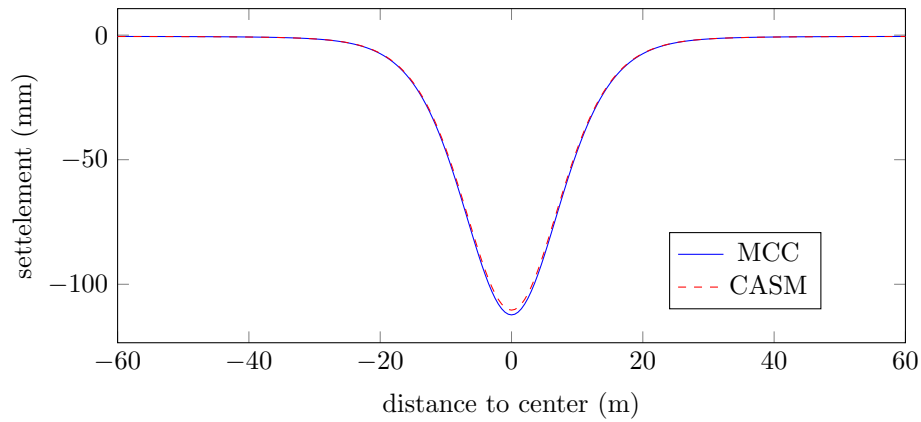


FIGURE 9 Tunnel excavation example: Settlement profile on top surface.

The settlement profile on the top surface, after the final step, is shown in Figure 9. As one shall expect, the results of MCC and CASM is very closed, due to the yield surfaces are matched.

In terms of convergence, the classical one-step algorithm fails for both MCC and CASM in the loading step when the traction is reduced. In the implicit sub-stepping algorithm, a total of 70 sub-steps for MCC and 392 sub-steps for CASM is required at those failed plastic points, recorded in the one-step analysis. The statistics of the sub-stepping algorithm are summarized in Table 2. In the table, PP denotes the plastic point, and SPP is the plastic point where the sub-stepping is required. The average number of sub-steps is computed by summing all number of sub-steps at SPP and divide by the number of SPPs.

Traction	MCC					CASM				
	No. of PP	No. of SPP	No. of sub-steps			No. of PP	No. of SPP	No. of sub-steps		
			Min.	Avg.	Max.			Min.	Avg.	Max.
70 %	45450	0	0	0	0	45450	0	0	0	0
40 %	45450	13	2	5.4	32	45450	87	2	4.5	16
26.67 %	45450	0	0	0	0	45450	0	0	0	0
13.33 %	45450	0	0	0	0	45450	0	0	0	0
0 %	45450	0	0	0	0	45450	0	0	0	0

TABLE 2 Excavation of a soil block: Displacements at the reference point A and the convergence of the implicit sub-stepping integration algorithm for different number of lifts.

In this example, the sub-stepping integration is required only in the step where the reduced traction occurs. Although the number of SPP is not high, it is crucial for the continuation of the analysis where one-step algorithm fails and cannot continue.

4 | CONCLUSIONS

This paper presents an implicit sub-stepping algorithm that greatly improves the computability of the critical state soil models. The sub-stepping stress integration is not new, nevertheless this is the first time a sub-stepping algorithm is fully linearized to be used with the implicit Newton-Raphson iteration for the critical state models, particularly for the popular Modified Cam-Clay and Clay-And-Sand models. The validation examples show that the sub-stepping integration algorithm can reproduce the analytical solution and the results exhibit quadratic convergence behaviour. In addition, the implicit sub-stepping algorithm is able to integrate the plastic points where the traditional one-step scheme fails. This greatly enhances the robustness of the critical state models and further promotes the usage of critical state models in geotechnical analysis. The implicit sub-stepping integration scheme can be extended to other soil models based on critical state concept, such as bounding Cam-Clay model, Barcelona-Basic model, etc, and will be the subject for future research.

4.1 | Acknowledgements

This presented work was conducted in the framework of the Collaborative Research Project SFB 837 "Interaction Modeling in Mechanized Tunneling", financed by the German Research Foundation (DFG) (Project number 77309832). The authors would like to thank the DFG for the support of this project.

References

1. Roscoe K, Schofield A. Mechanical behaviour of an idealised 'wet' clay. In: ; 1963; Wiesbaden.
2. Schofield A, Wroth P. *Critical State Soil Mechanics*. London: McGraw-Hill . 1968.
3. Roscoe K, Burland J. On the generalized stress strain behavior of wet clay. In: Heyman J, Leckie FA., eds. *Engineering Plasticity* Cambridge University Press; 1968; Cambridge: 535–609.
4. Gens A, Potts D. Critical state models in computational geomechanics. *Engineering Computations* 1988; 5: 178–197.
5. Yu H. CASM: A unified state parameter model for clay and sand. *International Journal for Numerical and Analytical Methods in Geomechanics* 1998; 48: 773–778.
6. Yu HS, Khong C, Wang J. A unified plasticity model for cyclic behaviour of clay and sand. *Mechanics Research Communications* 2007; 34(2): 97–114.
7. Simo J, Hughes T. *Computational Inelasticity*. Berlin: Springer . 1998.

8. Simo J, Taylor R. A return mapping algorithm for plane stress elastoplasticity. *International Journal of Numerical Methods in Engineering* 1986; 22(3): 649–670.
9. Borja R. Cam-Clay plasticity. Part I: Implicit integration of elasto-plastic constitutive relations. *Computer Methods in Applied Mechanics and Engineering* 1990; 78: 49–72.
10. Simo J, Meschke G. A New Class of Algorithms for Classical Plasticity Extended to Finite Strains. Application to Geomaterials. *Computational Mechanics* 1993; 11: 253–278.
11. Borja RI, Lin CH, Montáns FJ. Cam-Clay plasticity, Part IV: Implicit integration of anisotropic bounding surface model with nonlinear hyperelasticity and ellipsoidal loading function. *Computer Methods in Applied Mechanics and Engineering* 2001; 190(26–27): 3293–3323.
12. Borja RI, Choo J. Cam-Clay plasticity, Part VIII: A constitutive framework for porous materials with evolving internal structure. *Computer Methods in Applied Mechanics and Engineering* 2016; 309: 653–679.
13. Borja RI. Cam-Clay plasticity, Part V: A mathematical framework for three-phase deformation and strain localization analyses of partially saturated porous media. *Computer Methods in Applied Mechanics and Engineering* 2004; 193(48–51): 5301–5338.
14. Sloan SW. Substepping schemes for the numerical integration of elastoplastic stress-strain relations. *International Journal for Numerical Methods in Engineering* 1987; 24(5): 893–911.
15. Sloan SW, Abbo AJ, Sheng D. Refined explicit integration of elastoplastic models with automatic error control. *Engineering Computations* 2001; 18: 121–194.
16. Sheng D, Sloan SW. Load stepping schemes for critical state models. *International Journal for Numerical Methods in Engineering* 2001; 50(1): 67–93.
17. Zhao J, Sheng D, Rouainia M, Sloan SW. Explicit stress integration of complex soil models. *International Journal for Numerical and Analytical Methods in Geomechanics* 2005; 29(12): 1209–1229.
18. Abbo AJ, Sloan SW. An Automatic Load Stepping Algorithm with Error Control. *International Journal for Numerical Methods in Engineering* 1996; 39(10): 1737–1759.
19. Crisfield M. *Nonlinear Finite Element Analysis of Solids and Structures*. 1. John Wiley & sons. 1. ed. 1991.
20. Pérez-Fouget A, Rodríguez-Ferran A, Huerta A. Consistent tangent matrices for substepping schemes. *Computational Methods in Applied Mechanics and Engineering* 2001; 190(7): 4627–4647.

21. Roscoe K, Schofield A, Wroth C. On the yielding of soils. *Geotechnique* 1958; 8(1): 22-53.
22. Wood D. *Soil behaviour and critical state soil mechanics*. Cambridge: Cambridge University Press . 1990.
23. Borja R. Cam-Clay plasticity. Part II: Implicit integration of constitutive equation based on a nonlinear elastic stress predictor. *Computer Methods in Applied Mechanics and Engineering* 1991; 88: 225–240.
24. Perić D. Analytical solutions for a three-invariant Cam clay model subjected to drained loading histories. *International Journal for Numerical and Analytical Methods in Geomechanics* 2006; 30(5): 363–387.
25. Mikola RG. ADONIS: A free finite element analysis software with an interactive graphical user interface for geoengineers. In: ; 2017.

How to cite this article: Hoang-Giang Bui, Günther Meschke (2020), Implicit Integration with Sub-stepping Scheme for Critical State Models, *International Journal for Numerical Methods in Engineering*, xxx;xx:xx-xx.

APPENDIX

A LINEARIZATION OF THE ONE-STEP SCHEME, MODIFIED CAM-CLAY MODEL

Taking the linearization of (8) and (10), one obtains:

$$\frac{\partial p}{\partial \Delta \epsilon} = \frac{1+e}{\kappa} p \frac{\partial \Delta \epsilon_v^e}{\partial \Delta \epsilon}, \quad (\text{A1})$$

$$\frac{\partial p_c}{\partial \Delta \epsilon} = \theta p_c \left[\Delta \phi \left(2 \frac{\partial p}{\partial \Delta \epsilon} - \frac{\partial p_c}{\partial \Delta \epsilon} \right) + (2p - p_c) \frac{\partial \Delta \phi}{\partial \Delta \epsilon} \right]. \quad (\text{A2})$$

Equation (A2) is equivalent to:

$$\frac{\partial p_c}{\partial \Delta \epsilon} = \frac{\theta p_c}{1 + \theta p_c \Delta \phi} \left[2 \Delta \phi \frac{\partial p}{\partial \Delta \epsilon} + (2p - p_c) \frac{\partial \Delta \phi}{\partial \Delta \epsilon} \right]. \quad (\text{A3})$$

It is noted that $\Delta \epsilon_v^p = \Delta \phi (2p - p_c)$ and $\Delta \epsilon_v^e = \Delta \epsilon_v - \Delta \phi (2p - p_c)$, hence:

$$\frac{\partial \Delta \epsilon_v^e}{\partial \Delta \epsilon} = \mathbf{I} - \Delta \phi \left(2 \frac{\partial p}{\partial \Delta \epsilon} - \frac{\partial p_c}{\partial \Delta \epsilon} \right) - (2p - p_c) \frac{\partial \Delta \phi}{\partial \Delta \epsilon}. \quad (\text{A4})$$

Substituting (A4) and (A3) into (A1) leads to:

$$\left(1 + \frac{1+e}{\kappa} p \frac{2 \Delta \phi}{1 + \theta p_c \Delta \phi} \right) \frac{\partial p}{\partial \Delta \epsilon} = \frac{1+e}{\kappa} p \left[\mathbf{I} - \frac{2p - p_c}{1 + \theta p_c \Delta \phi} \frac{\partial \Delta \phi}{\partial \Delta \epsilon} \right]. \quad (\text{A5})$$

Equation (A5) can be rewritten as:

$$\frac{\partial p}{\partial \Delta \epsilon} = \mathbf{A}_1 + a_1 \frac{\partial \Delta \phi}{\partial \Delta \epsilon}, \quad K = \frac{1+e}{\kappa} p, \quad a_2 = 1 + (\theta p_c + 2K) \Delta \phi, \quad \mathbf{A} = \mathbf{A}_1 = \frac{1 + \theta p_c \Delta \phi}{a_2} K \mathbf{I}, \quad a = a_1 = -\frac{2p - p_c}{a_2} K. \quad (\text{A6})$$

Replaces (A6) into (A3), one obtains:

$$\frac{\partial p_c}{\partial \Delta \epsilon} = \mathbf{B}_1 + b_1 \frac{\partial \Delta \phi}{\partial \Delta \epsilon}, \quad \mathbf{B} = \mathbf{B}_1 = \frac{2\theta p_c \Delta \phi}{a_2} \mathbf{K} \mathbf{I}, \quad b = b_1 = \frac{2p - p_c}{a_2} \theta p_c. \quad (\text{A7})$$

The deviatoric pressure reads:

$$\mathbf{s} = \eta (\mathbf{s}_n + 2\bar{\mu} \Delta \epsilon_d), \quad \bar{\mu} = \frac{p - p_n}{\Delta \epsilon_v^e} r, \quad \eta = \left(1 + 6\bar{\mu} \frac{\Delta \phi}{M^2} \right)^{-1}. \quad (\text{A8})$$

Taking the linearization of (A8) with respect to $\Delta \epsilon$, one obtains:

$$\frac{\partial \mathbf{s}}{\partial \Delta \epsilon} = (\mathbf{s}_n + 2\bar{\mu} \Delta \epsilon_d) \otimes \frac{\partial \eta}{\partial \Delta \epsilon} + 2\eta \Delta \epsilon_d \otimes \frac{\partial \bar{\mu}}{\partial \Delta \epsilon} + 2\eta \bar{\mu} \frac{\partial \Delta \epsilon_d}{\partial \Delta \epsilon}. \quad (\text{A9})$$

In (A9), this relation holds: $\frac{\partial \Delta \epsilon_d}{\partial \Delta \epsilon} = \mathbb{I}_d = \mathbb{I} - \frac{1}{3} \mathbf{I} \otimes \mathbf{I}$, where \mathbb{I} is the fourth-order identity tensor. The linearization $\frac{\partial \bar{\mu}}{\partial \Delta \epsilon}$ and $\frac{\partial \eta}{\partial \Delta \epsilon}$ come as following:

$$\frac{\partial \bar{\mu}}{\partial \Delta \epsilon} = \mathbf{D}_1 + d_1 \frac{\partial \Delta \phi}{\partial \Delta \epsilon}, \quad \mathbf{D}_1 = \frac{Kr - \bar{\mu}}{K \Delta \epsilon_v^e} \mathbf{A}_1, \quad d_1 = \frac{Kr - \bar{\mu}}{K \Delta \epsilon_v^e} a_1, \quad (\text{A10})$$

$$\frac{\partial \eta}{\partial \Delta \epsilon} = \mathbf{D}_2 + d_2 \frac{\partial \Delta \phi}{\partial \Delta \epsilon}, \quad \mathbf{D}_2 = -6\eta^2 \frac{\Delta \phi}{M^2} \mathbf{D}_1, \quad d_2 = -\frac{6\eta^2}{M^2} (\Delta \phi d_1 + \bar{\mu}). \quad (\text{A11})$$

Substituting (A10) and (A11) into (A9) results in $\frac{\partial \mathbf{s}}{\partial \Delta \epsilon}$:

$$\frac{\partial \mathbf{s}}{\partial \Delta \epsilon} = \mathbb{D} + \mathbf{D}_3 \otimes \frac{\partial \Delta \phi}{\partial \Delta \epsilon}, \quad (\text{A12})$$

In which

$$\mathbb{D} = \mathbf{s}_n \otimes \mathbf{D}_2 + \Delta \epsilon_d \otimes 2(\bar{\mu} \mathbf{D}_2 + \eta \mathbf{D}_1) + 2\eta \bar{\mu} \mathbb{I}_d,$$

$$\mathbf{D} = \mathbf{D}_3 = d_2 \mathbf{s}_n + 2(\bar{\mu} d_2 + \eta d_1) \Delta \epsilon_d. \quad (\text{A13})$$

B LINEARIZATION OF THE SUB-STEPPING SCHEME, MODIFIED CAM-CLAY MODEL

Taking linearization of (8) and (10) for the sub-step $(k+1)$, with the remark that linearization of ${}^k p$ and ${}^k p_c$ do not vanish, one obtains:

$$\frac{\partial {}^{k+1} p}{\partial \Delta \epsilon} = \frac{{}^{k+1} p}{{}^k p} \frac{\partial {}^k p}{\partial \Delta \epsilon} + \frac{1 + e_{k+1}}{\kappa} p \frac{\partial {}^{k+1} \Delta \epsilon_v^e}{\partial \Delta \epsilon}, \quad (\text{B14})$$

and

$$\frac{\partial {}^{k+1} p_c}{\partial \Delta \epsilon} = \frac{{}^{k+1} p_c}{{}^k p_c} \frac{\partial {}^k p_c}{\partial \Delta \epsilon} + \theta {}^{k+1} p_c \left[\Delta \phi \left(2 \frac{\partial {}^{k+1} p}{\partial \Delta \epsilon} - \frac{\partial {}^{k+1} p_c}{\partial \Delta \epsilon} \right) + (2 {}^{k+1} p - {}^{k+1} p_c) \frac{\partial \Delta \phi}{\partial \Delta \epsilon} \right]. \quad (\text{B15})$$

It is noted that ${}^{k+1} \Delta \epsilon_v^e = {}^{k+1} \Delta \epsilon_v - \Delta \phi (2 {}^{k+1} p - {}^{k+1} p_c)$, hence:

$$\frac{\partial {}^{k+1} \Delta \epsilon_v^e}{\partial \Delta \epsilon} = \alpha_{k+1} \mathbf{I} - \Delta \phi \left(2 \frac{\partial {}^{k+1} p}{\partial \Delta \epsilon} - \frac{\partial {}^{k+1} p_c}{\partial \Delta \epsilon} \right) - (2 {}^{k+1} p - {}^{k+1} p_c) \frac{\partial \Delta \phi}{\partial \Delta \epsilon}. \quad (\text{B16})$$

Using (B16) and solve (B14) and (B15) with respect to variable $\frac{\partial^{k+1}p}{\partial\Delta\varepsilon}$ and $\frac{\partial^{k+1}p_c}{\partial\Delta\varepsilon}$ leads to:

$$\frac{\partial^{k+1}p}{\partial\Delta\varepsilon} = \mathbf{A}_1 + a_1 \frac{\partial\Delta\phi}{\partial\Delta\varepsilon}, \quad \frac{\partial^{k+1}p_c}{\partial\Delta\varepsilon} = \mathbf{B}_1 + b_1 \frac{\partial\Delta\phi}{\partial\Delta\varepsilon}. \quad (\text{B17})$$

In which

$$\mathbf{A} = \mathbf{A}_1 = \frac{1 + \theta^{k+1}p_c\Delta\phi}{a_2} \left(\frac{{}^{k+1}p}{k} \frac{\partial^k p}{\partial\Delta\varepsilon} + \alpha_{k+1} {}^{k+1}K\mathbf{I} \right) + \frac{{}^{k+1}K\Delta\phi}{{}^k p_c} \frac{\partial^k p_c}{\Delta\varepsilon},$$

$$a = a_1 = -\frac{2^{k+1}p - {}^{k+1}p_c}{{}^k p_c} {}^{k+1}K,$$

$$a_2 = 1 + (\theta^{k+1}p_c + 2^{k+1}K) \Delta\phi. \quad (\text{B18})$$

$$\mathbf{B} = \mathbf{B}_1 = \frac{2\theta^{k+1}p_c\Delta\phi}{a_2} \left(\frac{{}^{k+1}p}{k} \frac{\partial^k p}{\partial\Delta\varepsilon} + \alpha_{k+1} {}^{k+1}K\mathbf{I} \right) + \frac{1 + 2^{k+1}K\Delta\phi}{{}^k p_c} \frac{\partial^k p_c}{\Delta\varepsilon}, \quad (\text{B19})$$

$$b = b_1 = \frac{\theta^{k+1}p_c}{{}^k p_c} (2^{k+1}p - {}^{k+1}p_c), \quad (\text{B20})$$

$${}^{k+1}K = \frac{1 + e^{k+1}p}{\kappa}. \quad (\text{B21})$$

From Equation (B14):

$$\frac{\partial^{k+1}\Delta\varepsilon_v^e}{\partial\Delta\varepsilon} = \frac{1}{{}^{k+1}K} \left(\frac{\partial^{k+1}p}{\partial\Delta\varepsilon} - \frac{{}^{k+1}p}{k} \frac{\partial^k p}{\partial\Delta\varepsilon} \right) = \mathbf{C}_1 + c_1 \frac{\partial\Delta\phi}{\partial\Delta\varepsilon}, \quad \mathbf{C}_1 = \frac{1}{{}^{k+1}K} \left(\mathbf{A}_1 - \frac{{}^{k+1}p}{k} \frac{\partial^k p}{\partial\Delta\varepsilon} \right), \quad c_1 = \frac{a_1}{{}^{k+1}K} \quad (\text{B22})$$

The deviatoric pressure reads:

$${}^{k+1}\mathbf{s} = \eta ({}^k\mathbf{s} + 2\bar{\mu} {}^{k+1}\Delta\varepsilon_d), \quad \bar{\mu} = \frac{{}^{k+1}p - {}^k p}{{}^{k+1}\Delta\varepsilon_v^e} r, \quad \eta = \left(1 + 6\bar{\mu} \frac{\Delta\phi}{M^2} \right)^{-1}. \quad (\text{B23})$$

It is therefore:

$$\frac{\partial\bar{\mu}}{\partial\Delta\varepsilon} = \frac{r}{{}^{k+1}\Delta\varepsilon_v^e} \left(\frac{\partial^{k+1}p}{\partial\Delta\varepsilon} - \frac{\partial^k p}{\partial\Delta\varepsilon} \right) - \frac{\bar{\mu}}{{}^{k+1}\Delta\varepsilon_v^e} \frac{\partial^{k+1}\Delta\varepsilon_v^e}{\partial\Delta\varepsilon}. \quad (\text{B24})$$

Replace (B14) and (B22) into (B24), one obtains:

$$\frac{\partial\bar{\mu}}{\partial\Delta\varepsilon} = \mathbf{D}_1 + d_1 \frac{\partial\Delta\phi}{\partial\Delta\varepsilon}, \quad \mathbf{D}_1 = \frac{r\mathbf{A}_1 - \bar{\mu}\mathbf{C}_1}{{}^{k+1}\Delta\varepsilon_v^e} - \frac{r}{{}^{k+1}\Delta\varepsilon_v^e} \frac{\partial^k p}{\partial\Delta\varepsilon}, \quad d_1 = \frac{ra_1 - \bar{\mu}c_1}{{}^{k+1}\Delta\varepsilon_v^e}. \quad (\text{B25})$$

The derivation of $\frac{\partial\eta}{\partial\Delta\varepsilon}$ is similar to (A11), which reads:

$$\frac{\partial\eta}{\partial\Delta\varepsilon} = -\frac{6\eta^2}{M^2} \left(\Delta\phi \frac{\partial\bar{\mu}}{\partial\Delta\varepsilon} + \bar{\mu} \frac{\partial\Delta\phi}{\partial\Delta\varepsilon} \right) = \mathbf{D}_2 + d_2 \frac{\partial\Delta\phi}{\partial\Delta\varepsilon}, \quad \mathbf{D}_2 = -\frac{6\eta^2\Delta\phi}{M^2} \mathbf{D}_1, \quad d_2 = -\frac{6\eta^2}{M^2} (\Delta\phi d_1 + \bar{\mu}). \quad (\text{B26})$$

The linearization of deviatoric pressure ${}^{k+1}\mathbf{s}$ follows by:

$$\frac{\partial^{k+1}\mathbf{s}}{\partial\Delta\varepsilon} = ({}^k\mathbf{s} + 2\bar{\mu} {}^{k+1}\Delta\varepsilon_d) \otimes \frac{\partial\eta}{\partial\Delta\varepsilon} + \eta \frac{\partial^k \mathbf{s}}{\partial\Delta\varepsilon} + 2\eta {}^{k+1}\Delta\varepsilon_d \otimes \frac{\partial\bar{\mu}}{\partial\Delta\varepsilon} + 2\eta\bar{\mu} \frac{\partial^{k+1}\Delta\varepsilon_d}{\partial\Delta\varepsilon} = \mathbb{D} + \mathbf{D}_3 \otimes \frac{\Delta\phi}{\Delta\varepsilon}, \quad (\text{B27})$$

In which

$$\begin{aligned}\mathbb{D} &= \left({}^k\mathbf{s} + 2\bar{\mu}^{k+1}\Delta\boldsymbol{\varepsilon}_d \right) \otimes \mathbf{D}_2 + \eta \frac{\partial {}^k\mathbf{s}}{\partial \Delta\boldsymbol{\varepsilon}} + 2\eta^{k+1}\Delta\boldsymbol{\varepsilon}_d \otimes \mathbf{D}_1 + 2\alpha_{k+1}\eta\bar{\mu}\mathbb{1}_d, \\ \mathbf{D} &= \mathbf{D}_3 = d_2 \left({}^k\mathbf{s} + 2\bar{\mu}^{k+1}\Delta\boldsymbol{\varepsilon}_d \right) + 2\eta d_1^{k+1}\Delta\boldsymbol{\varepsilon}_d.\end{aligned}\quad (\text{B28})$$

C SOLUTION OF THE LOCAL NONLINEAR SYSTEM, CASM MODEL

In order to derive the solution of the local nonlinear system, necessary derivatives of the yield function and plastic potential are given to support for further derivation:

$$f_p = \frac{\partial f}{\partial p} = -\frac{Nq^N}{M^N p^{N+1}} + \frac{1}{p \ln R}, \quad f_q = \frac{\partial f}{\partial q} = \frac{Nq^{N-1}}{M^N p^N}, \quad f_{p_c} = \frac{\partial f}{\partial p_c} = -\frac{1}{p_c \ln R}, \quad (\text{C29})$$

$$g_p = \frac{\partial g}{\partial p} = 3\frac{3+2M}{3p+2q} - 3\frac{3-M}{3p-q}, \quad g_q = \frac{\partial g}{\partial q} = 2\frac{3+2M}{3p+2q} + \frac{3-M}{3p-q}, \quad (\text{C30})$$

$$g_{pp} = \frac{\partial^2 g}{\partial p^2} = -9\frac{3+2M}{(3p+2q)^2} + 9\frac{3-M}{(3p-q)^2}, \quad g_{qq} = \frac{\partial^2 g}{\partial q^2} = -4\frac{3+2M}{(3p+2q)^2} + \frac{3-M}{(3p-q)^2}, \quad (\text{C31})$$

$$g_{pq} = \frac{\partial^2 g}{\partial p \partial q} = -6\frac{3+2M}{(3p+2q)^2} - 3\frac{3-M}{(3p-q)^2}. \quad (\text{C32})$$

Additional terms are defined as:

$$K = \frac{1+e}{\kappa}p, \quad \bar{\mu} = Kr, \quad \eta = \left(1 + 3\bar{\mu} \frac{\Delta\phi}{q} g_q \right)^{-1}, \quad \hat{\mathbf{n}} = \frac{\mathbf{s}_n + 2\bar{\mu}\Delta\boldsymbol{\varepsilon}_d}{\|\mathbf{s}_n + 2\bar{\mu}\Delta\boldsymbol{\varepsilon}_d\|}. \quad (\text{C33})$$

The flow rule reads:

$$\Delta\boldsymbol{\varepsilon}_v^p = \Delta\phi g_p, \quad \Delta\boldsymbol{\varepsilon}_v^e = \Delta\boldsymbol{\varepsilon}_v - \Delta\boldsymbol{\varepsilon}_v^p, \quad \Delta\boldsymbol{\varepsilon}_d^p = \sqrt{\frac{3}{2}}\Delta\phi g_q \hat{\mathbf{n}}, \quad \Delta\boldsymbol{\varepsilon}_d^e = \Delta\boldsymbol{\varepsilon}_d - \Delta\boldsymbol{\varepsilon}_d^p. \quad (\text{C34})$$

The derivatives of $\bar{\mu}$ and η read:

$$\bar{\mu}_p = \frac{\partial \bar{\mu}}{\partial p} = \frac{1}{\Delta\boldsymbol{\varepsilon}_v^e} (r + \bar{\mu}\Delta\phi g_{pp}), \quad \bar{\mu}_q = \frac{\partial \bar{\mu}}{\partial q} = \frac{\bar{\mu}}{\Delta\boldsymbol{\varepsilon}_v^e} \Delta\phi g_{pq}, \quad \bar{\mu}_{p_c} = \frac{\partial \bar{\mu}}{\partial p_c} = 0, \quad \bar{\mu}_{\Delta\phi} = \frac{\partial \bar{\mu}}{\partial \Delta\phi} = \frac{\bar{\mu}}{\Delta\boldsymbol{\varepsilon}_v^e} g_p, \quad (\text{C35})$$

$$\begin{aligned}\eta_p &= \frac{\partial \eta}{\partial p} = -3\frac{\Delta\phi}{q} (\bar{\mu}_p g_q + \bar{\mu} g_{pq}) \eta^2, \quad \eta_q = \frac{\partial \eta}{\partial q} = -3\frac{\Delta\phi}{q} \left(\left(\bar{\mu}_q - \frac{\bar{\mu}}{q} \right) g_q + \bar{\mu} g_{qq} \right) \eta^2, \\ \bar{\eta}_{p_c} &= \frac{\partial \eta}{\partial p_c} = 0, \quad \bar{\eta}_{\Delta\phi} = \frac{\partial \eta}{\partial \Delta\phi} = -\frac{3}{q} (\bar{\mu} + \bar{\mu}_{\Delta\phi} \Delta\phi) g_q \eta^2.\end{aligned}\quad (\text{C36})$$

The necessary derivatives to solver local system (8) (9) (10) (11) are given as follow:

$$h_{1,1} = \frac{\partial h_1}{\partial p} = 1 + K\Delta\phi g_{pp}, \quad h_{1,2} = \frac{\partial h_1}{\partial q} = K\Delta\phi g_{pq}, \quad h_{1,3} = \frac{\partial h_1}{\partial p_c} = 0, \quad h_{1,4} = \frac{\partial h_1}{\partial \Delta\phi} = Kg_p.$$

$$h_{2,1} = \frac{\partial h_2}{\partial p} = -\sqrt{\frac{3}{2}}\eta_p \|s_n + 2\bar{\mu}\Delta\epsilon_d\| - 2\sqrt{\frac{3}{2}}\eta\bar{\mu}_p \hat{\mathbf{n}} : \Delta\epsilon_d, \quad h_{2,2} = \frac{\partial h_2}{\partial q} = 1 - \sqrt{\frac{3}{2}}\eta_q \|s_n + 2\bar{\mu}\Delta\epsilon_d\| - 2\sqrt{\frac{3}{2}}\eta\bar{\mu}_q \hat{\mathbf{n}} : \Delta\epsilon_d,$$

$$h_{2,3} = \frac{\partial h_2}{\partial p_c} = -2\sqrt{\frac{3}{2}}\eta\bar{\mu}_{p_c} \hat{\mathbf{n}} : \Delta\epsilon_d, \quad h_{2,4} = \frac{\partial h_2}{\partial \Delta\phi} = -\sqrt{\frac{3}{2}}\eta_{\Delta\phi} \|s_n + 2\bar{\mu}\Delta\epsilon_d\| - 2\sqrt{\frac{3}{2}}\eta\bar{\mu}_{\Delta\phi} \hat{\mathbf{n}} : \Delta\epsilon_d,$$

$$h_{3,1} = \frac{\partial h_3}{\partial p} = -\theta p_c \Delta\phi g_{pp}, \quad h_{3,2} = \frac{\partial h_3}{\partial q} = -\theta p_c \Delta\phi g_{pq}, \quad h_{3,3} = \frac{\partial h_3}{\partial p_c} = 1, \quad h_{3,4} = \frac{\partial h_3}{\partial \Delta\phi} = -\theta p_c g_p,$$

$$h_{4,1} = \frac{\partial h_4}{\partial p} = f_p, \quad h_{4,2} = \frac{\partial h_4}{\partial q} = f_q, \quad h_{4,3} = \frac{\partial h_4}{\partial p_c} = f_{p_c}, \quad h_{4,4} = \frac{\partial h_4}{\partial \Delta\phi} = 0.$$

D LINEARIZATION OF THE ONE-STEP SCHEME, CASM MODEL

Taking the linearization of (8), one obtains:

$$\frac{\partial p}{\partial \Delta\epsilon} = K \frac{\partial \Delta\epsilon_v^e}{\partial \Delta\epsilon}, \quad K = \frac{1+e}{\kappa} p. \quad (\text{D37})$$

It is noted that $\Delta\epsilon_v^e = \Delta\epsilon_v - \Delta\phi g_p$, hence:

$$\frac{\partial \Delta\epsilon_v^e}{\partial \Delta\epsilon} = \mathbf{I} - \Delta\phi g_{pp} \frac{\partial p}{\partial \Delta\epsilon} - \Delta\phi g_{pq} \frac{\partial q}{\partial \Delta\epsilon} - g_p \frac{\partial \Delta\phi}{\partial \Delta\epsilon}. \quad (\text{D38})$$

From (D37) and (D38), one can rewrite $\frac{\partial p}{\partial \Delta\epsilon}$ as dependent term of $\frac{\partial q}{\partial \Delta\epsilon}$ and $\frac{\partial \Delta\phi}{\partial \Delta\epsilon}$:

$$\frac{\partial p}{\partial \Delta\epsilon} = \mathbf{A}_1 + a_1 \frac{\partial \Delta\phi}{\partial \Delta\epsilon} + a_2 \frac{\partial q}{\partial \Delta\epsilon}, \quad \mathbf{A}_1 = a_3 K \mathbf{I},$$

$$a_1 = -a_3 K g_p, \quad a_2 = -a_3 K \Delta\phi g_{pq}, \quad a_3 = (1 + K \Delta\phi g_{pp})^{-1}. \quad (\text{D39})$$

Taking the linearization of (10):

$$\frac{\partial p_c}{\partial \Delta\epsilon} = \theta p_c \left(\mathbf{I} - \frac{\partial \Delta\epsilon_v^e}{\partial \Delta\epsilon} \right) = \mathbf{B}_1 + b_1 \frac{\partial \Delta\phi}{\partial \Delta\epsilon} + b_2 \frac{\partial q}{\partial \Delta\epsilon},$$

$$\mathbf{B}_1 = \frac{\theta p_c}{K} (K \mathbf{I} - \mathbf{A}_1), \quad b_1 = -\frac{\theta p_c}{K} a_1, \quad b_2 = -\frac{\theta p_c}{K} a_2. \quad (\text{D40})$$

The deviatoric pressure reads:

$$\mathbf{s} = \eta (\mathbf{s}_n + 2\bar{\mu}\Delta\epsilon_d), \quad \bar{\mu} = \frac{p - p_n}{\Delta\epsilon_v^e} r, \quad \eta = \left(1 + 3\bar{\mu} \frac{\Delta\phi}{q} g_q \right)^{-1}. \quad (\text{D41})$$

The linearization of $\bar{\mu}$ comes as follows:

$$\frac{\partial \bar{\mu}}{\partial \Delta\epsilon} = \mathbf{D}_1 + d_1 \frac{\partial \Delta\phi}{\partial \Delta\epsilon} + d_2 \frac{\partial q}{\partial \Delta\epsilon}, \quad \mathbf{D}_1 = \frac{Kr - \bar{\mu}}{K \Delta\epsilon_v^e} \mathbf{A}_1,$$

$$d_1 = \frac{Kr - \bar{\mu}}{K \Delta\epsilon_v^e} a_1, \quad d_2 = \frac{Kr - \bar{\mu}}{K \Delta\epsilon_v^e} a_2. \quad (\text{D42})$$

The linearization of η comes as follows:

$$\begin{aligned} \frac{\partial \eta}{\partial \Delta \epsilon} &= \mathbf{D}_2 + d_3 \frac{\partial \Delta \phi}{\partial \Delta \epsilon} + d_4 \frac{\partial q}{\partial \Delta \epsilon}, \quad \mathbf{D}_2 = -3\eta^2 \frac{\Delta \phi}{q} (g_q \mathbf{D}_1 + \bar{\mu} g_{pq} \mathbf{A}_1), \\ d_3 &= -3\eta^2 \left(\left[\frac{\Delta \phi}{q} d_1 + \frac{\bar{\mu}}{q} \right] g_q + \frac{\bar{\mu} \Delta \phi}{q} g_{pq} a_1 \right), \quad d_4 = -3\eta^2 \frac{\Delta \phi}{q} \left(\left[d_2 - \frac{\bar{\mu}}{q} \right] g_q + \bar{\mu} [g_{pq} a_2 + g_{qq}] \right). \end{aligned} \quad (\text{D43})$$

The linearization of \mathbf{s} comes as follows:

$$\begin{aligned} \frac{\partial \mathbf{s}}{\partial \Delta \epsilon} &= 2\eta \left(\bar{\mu} \mathbb{1}_d + \Delta \epsilon_d \otimes \frac{\partial \bar{\mu}}{\partial \Delta \epsilon} \right) + (\mathbf{s}_n + 2\bar{\mu} \Delta \epsilon_d) \otimes \frac{\partial \eta}{\partial \Delta \epsilon} = \mathbb{D}_1 + \mathbf{D}_3 \otimes \frac{\partial \Delta \phi}{\partial \Delta \epsilon} + \mathbf{D}_4 \otimes \frac{\partial q}{\partial \Delta \epsilon}, \\ \mathbb{D}_1 &= 2\eta \bar{\mu} \mathbb{1}_d + 2\eta \Delta \epsilon_d \otimes \mathbf{D}_1 + (\mathbf{s}_n + 2\bar{\mu} \Delta \epsilon_d) \otimes \mathbf{D}_2, \\ \mathbf{D}_3 &= d_3 \mathbf{s}_n + 2(\bar{\mu} d_3 + \eta d_1) \Delta \epsilon_d, \quad \mathbf{D}_4 = d_4 \mathbf{s}_n + 2(\bar{\mu} d_4 + \eta d_2) \Delta \epsilon_d. \end{aligned} \quad (\text{D44})$$

From the relation $2q \frac{\partial q}{\partial \Delta \epsilon} = 3\mathbf{s} : \frac{\partial \mathbf{s}}{\partial \Delta \epsilon}$, the linearization of q reduces to:

$$\frac{\partial q}{\partial \Delta \epsilon} = \mathbf{D}_5 + d_5 \frac{\partial \Delta \phi}{\partial \Delta \epsilon}, \quad \mathbf{D}_5 = \frac{3}{2} \frac{d_6}{q} \mathbf{s} : \mathbb{D}_1, \quad d_5 = \frac{3}{2} \frac{d_6}{q} \mathbf{s} : \mathbf{D}_3, \quad d_6 = \left(1 - \frac{3}{2} \frac{1}{q} \mathbf{s} : \mathbf{D}_4 \right)^{-1}. \quad (\text{D45})$$

Replacing (D45) back into (D39), (D40) and (D44), we obtain the dependency of linearization of p , p_c and \mathbf{s} on only $\frac{\partial \Delta \phi}{\partial \Delta \epsilon}$:

$$\begin{aligned} \frac{\partial p}{\partial \Delta \epsilon} &= \mathbf{A} + a \frac{\partial \Delta \phi}{\partial \Delta \epsilon}, \quad \mathbf{A} = \mathbf{A}_1 + a_2 \mathbf{D}_5, \quad a = a_1 + a_2 d_5, \\ \frac{\partial p_c}{\partial \Delta \epsilon} &= \mathbf{B} + b \frac{\partial \Delta \phi}{\partial \Delta \epsilon}, \quad \mathbf{B} = \mathbf{B}_1 + b_2 \mathbf{D}_5, \quad b = b_1 + b_2 d_5, \\ \frac{\partial \mathbf{s}}{\partial \Delta \epsilon} &= \mathbb{D} + \mathbf{D} \frac{\partial \Delta \phi}{\partial \Delta \epsilon}, \quad \mathbb{D} = \mathbb{D}_1 + \mathbf{D}_4 \otimes \mathbf{D}_5, \quad \mathbf{D} = \mathbf{D}_3 + d_5 \mathbf{D}_4. \end{aligned} \quad (\text{D46})$$

E LINEARIZATION OF THE SUB-STEPPING SCHEME, CASM MODEL

Taking linearization of (8) for the sub-step $(k+1)$, with the remark that linearization of ${}^k p$ does not vanish, one obtains:

$$\frac{\partial {}^{k+1} p}{\partial \Delta \epsilon} = \frac{{}^{k+1} p}{k p} \frac{\partial {}^k p}{\partial \Delta \epsilon} + {}^{k+1} K \frac{\partial {}^{k+1} \Delta \epsilon_v^e}{\partial \Delta \epsilon}, \quad {}^{k+1} K = \frac{1+e}{\kappa} {}^{k+1} p. \quad (\text{E47})$$

It is noted that ${}^{k+1} \Delta \epsilon_v^e = {}^{k+1} \Delta \epsilon_v - \Delta \phi g_p$, hence:

$$\frac{\partial {}^{k+1} \Delta \epsilon_v^e}{\partial \Delta \epsilon} = \alpha_{k+1} \mathbf{I} - \Delta \phi \left(g_{pp} \frac{\partial {}^{k+1} p}{\partial \Delta \epsilon} + g_{pq} \frac{\partial {}^{k+1} q}{\partial \Delta \epsilon} \right) - g_p \frac{\partial \Delta \phi}{\partial \Delta \epsilon}. \quad (\text{E48})$$

In Equation (E48) and further equations below, g_p , g_q , g_{pp} , g_{pq} and g_{qq} are evaluated at $({}^{k+1} p, {}^{k+1} q)$.

From (E47) and (E48), one can rewrite $\frac{\partial {}^{k+1} p}{\partial \Delta \epsilon}$ as dependent term of $\frac{\partial {}^{k+1} q}{\partial \Delta \epsilon}$ and $\frac{\partial \Delta \phi}{\partial \Delta \epsilon}$:

$$\begin{aligned} \frac{\partial {}^{k+1} p}{\partial \Delta \epsilon} &= \mathbf{A}_1 + a_1 \frac{\partial \Delta \phi}{\partial \Delta \epsilon} + a_2 \frac{\partial {}^{k+1} q}{\partial \Delta \epsilon}, \quad \mathbf{A}_1 = a_3 \left(\frac{{}^{k+1} p}{k p} \frac{\partial {}^k p}{\partial \Delta \epsilon} + \alpha_{k+1} {}^{k+1} K \mathbf{I} \right), \\ a_1 &= -a_3 {}^{k+1} K g_p, \quad a_2 = -a_3 {}^{k+1} K \Delta \phi g_{pq}, \quad a_3 = \left(1 + {}^{k+1} K \Delta \phi g_{pp} \right)^{-1}. \end{aligned} \quad (\text{E49})$$

Taking the linearization of (10):

$$\begin{aligned} \frac{\partial^{k+1} p_c}{\partial \Delta \epsilon} &= \frac{k+1}{k} p_c \frac{\partial^k p_c}{\partial \Delta \epsilon} + \theta^{k+1} p_c \left(\alpha_{k+1} \mathbf{I} - \frac{\partial^{k+1} \Delta \epsilon_v^e}{\partial \Delta \epsilon} \right) = \mathbf{B}_1 + b_1 \frac{\partial \Delta \phi}{\partial \Delta \epsilon} + b_2 \frac{\partial^{k+1} q}{\partial \Delta \epsilon}, \\ \mathbf{B}_1 &= \frac{k+1}{k} p_c \frac{\partial^k p_c}{\partial \Delta \epsilon} + \frac{\theta^{k+1} p_c}{k+1 K} \left(\alpha_{k+1}^{k+1} K \mathbf{I} + \frac{k+1}{k} p \frac{\partial^k p}{\partial \Delta \epsilon} - \mathbf{A}_1 \right), \quad b_1 = -\frac{\theta^{k+1} p_c}{k+1 K} a_1, \quad b_2 = -\frac{\theta^{k+1} p_c}{k+1 K} a_2. \end{aligned} \quad (\text{E50})$$

The deviatoric pressure reads:

$${}^{k+1} \mathbf{s} = \eta \left({}^k \mathbf{s} + 2\bar{\mu}^{k+1} \Delta \epsilon_d \right), \quad \bar{\mu} = \frac{k+1}{k+1} \frac{p - k}{\Delta \epsilon_v^e} r, \quad \eta = \left(1 + 3\bar{\mu} \frac{\Delta \phi}{k+1} g_q \right)^{-1}. \quad (\text{E51})$$

The linearization of $\bar{\mu}$ comes as follows:

$$\begin{aligned} \frac{\partial \bar{\mu}}{\partial \Delta \epsilon} &= \mathbf{D}_1 + d_1 \frac{\partial \Delta \phi}{\partial \Delta \epsilon} + d_2 \frac{\partial^{k+1} q}{\partial \Delta \epsilon}, \quad \mathbf{D}_1 = \frac{k+1}{k+1} \frac{K r - \bar{\mu}}{K^{k+1} \Delta \epsilon_v^e} \mathbf{A}_1 - \frac{1}{k+1 \Delta \epsilon_v^e} \left(r - \frac{\bar{\mu}}{k+1} \frac{k+1}{K} \frac{p}{k} \right) \frac{\partial^k p}{\partial \Delta \epsilon}, \\ d_1 &= \frac{k+1}{k+1} \frac{K r - \bar{\mu}}{K^{k+1} \Delta \epsilon_v^e} a_1, \quad d_2 = \frac{k+1}{k+1} \frac{K r - \bar{\mu}}{K^{k+1} \Delta \epsilon_v^e} a_2. \end{aligned} \quad (\text{E52})$$

The linearization of η comes as follows:

$$\begin{aligned} \frac{\partial \eta}{\partial \Delta \epsilon} &= \mathbf{D}_2 + d_3 \frac{\partial \Delta \phi}{\partial \Delta \epsilon} + d_4 \frac{\partial^{k+1} q}{\partial \Delta \epsilon}, \quad \mathbf{D}_2 = -3\eta^2 \frac{\Delta \phi}{k+1} (g_q \mathbf{D}_1 + \bar{\mu} g_{pq} \mathbf{A}_1), \\ d_3 &= -3\eta^2 \left(\left[\frac{\Delta \phi}{k+1} d_1 + \frac{\bar{\mu}}{k+1} \right] g_q + \frac{\bar{\mu} \Delta \phi}{k+1} g_{pq} a_1 \right), \quad d_4 = -3\eta^2 \frac{\Delta \phi}{k+1} \left(\left[d_2 - \frac{\bar{\mu}}{k+1} \right] g_q + \bar{\mu} [g_{pq} a_2 + g_{qq}] \right). \end{aligned} \quad (\text{E53})$$

The linearization of ${}^{k+1} \mathbf{s}$ comes as follows:

$$\begin{aligned} \frac{\partial^{k+1} \mathbf{s}}{\partial \Delta \epsilon} &= \eta \left(\frac{\partial^k \mathbf{s}}{\partial \Delta \epsilon} + 2\alpha_{k+1} \bar{\mu} \mathbb{1}_d + 2^{k+1} \Delta \epsilon_d \otimes \frac{\partial \bar{\mu}}{\partial \Delta \epsilon} \right) + ({}^k \mathbf{s} + 2\bar{\mu}^{k+1} \Delta \epsilon_d) \otimes \frac{\partial \eta}{\partial \Delta \epsilon} = \mathbb{D}_1 + \mathbf{D}_3 \otimes \frac{\partial \Delta \phi}{\partial \Delta \epsilon} + \mathbf{D}_4 \otimes \frac{\partial^{k+1} q}{\partial \Delta \epsilon}, \\ \mathbb{D}_1 &= \eta \left(\frac{\partial^k \mathbf{s}}{\partial \Delta \epsilon} + 2\alpha_{k+1} \bar{\mu} \mathbb{1}_d + 2^{k+1} \Delta \epsilon_d \otimes \mathbf{D}_1 \right) + ({}^k \mathbf{s} + 2\bar{\mu}^{k+1} \Delta \epsilon_d) \otimes \mathbf{D}_2, \\ \mathbf{D}_3 &= d_3 {}^k \mathbf{s} + 2(\bar{\mu} d_3 + \eta d_1) {}^{k+1} \Delta \epsilon_d, \quad \mathbf{D}_4 = d_4 {}^k \mathbf{s} + 2(\bar{\mu} d_4 + \eta d_2) {}^{k+1} \Delta \epsilon_d. \end{aligned} \quad (\text{E54})$$

From the relation $2^{k+1} q \frac{\partial^{k+1} q}{\partial \Delta \epsilon} = 3^{k+1} \mathbf{s} : \frac{\partial^{k+1} \mathbf{s}}{\partial \Delta \epsilon}$, the linearization of ${}^{k+1} q$ reduces to:

$$\frac{\partial^{k+1} q}{\partial \Delta \epsilon} = \mathbf{D}_5 + d_5 \frac{\partial \Delta \phi}{\partial \Delta \epsilon}, \quad \mathbf{D}_5 = \frac{3}{2} \frac{d_6}{k+1} {}^{k+1} \mathbf{s} : \mathbb{D}_1, \quad d_5 = \frac{3}{2} \frac{d_6}{k+1} {}^{k+1} \mathbf{s} : \mathbf{D}_3, \quad d_6 = \left(1 - \frac{3}{2} \frac{1}{k+1} {}^{k+1} \mathbf{s} : \mathbf{D}_4 \right)^{-1}. \quad (\text{E55})$$

Replacing (E55) back into (E49), (E50) and (E54), we obtain the dependency of linearization of p , p_c and \mathbf{s} on only $\frac{\partial \Delta \phi}{\partial \Delta \epsilon}$:

$$\begin{aligned} \frac{\partial^{k+1} p}{\partial \Delta \epsilon} &= \mathbf{A} + a \frac{\partial \Delta \phi}{\partial \Delta \epsilon}, \quad \mathbf{A} = \mathbf{A}_1 + a_2 \mathbf{D}_5, \quad a = a_1 + a_2 d_5, \\ \frac{\partial^{k+1} p_c}{\partial \Delta \epsilon} &= \mathbf{B} + b \frac{\partial \Delta \phi}{\partial \Delta \epsilon}, \quad \mathbf{B} = \mathbf{B}_1 + b_2 \mathbf{D}_5, \quad b = b_1 + b_2 d_5, \\ \frac{\partial^{k+1} \mathbf{s}}{\partial \Delta \epsilon} &= \mathbb{D} + \mathbf{D} \frac{\partial \Delta \phi}{\partial \Delta \epsilon}, \quad \mathbb{D} = \mathbb{D}_1 + \mathbf{D}_4 \otimes \mathbf{D}_5, \quad \mathbf{D} = \mathbf{D}_3 + d_5 \mathbf{D}_4. \end{aligned} \quad (\text{E56})$$

F ANALYTICAL SOLUTION OF CASM MODEL SUBJECTED TO DRAINED PROPORTIONAL STRESS PATH

In the proportional loading scheme, the loading is governed by:

$$\dot{q} = k\dot{p}, \quad k = \text{const.} \quad (\text{F57})$$

For further derivation, we denote $\beta = \frac{q}{p}$, subsequently:

$$q = \beta p, \quad \dot{q} = \dot{\beta} p + \beta \dot{p}. \quad (\text{F58})$$

Because of Equation (F57), one can deduce

$$k\dot{p} = \dot{\beta} p + \beta \dot{p} \quad \Rightarrow \quad \frac{\dot{p}}{p} = \frac{\dot{\beta}}{k - \beta}. \quad (\text{F59})$$

F.1 Solution for volumetric strain

F.1.1 Elastic domain

The Equations (2) and (3) leads to:

$$\dot{\epsilon}_v^e = \frac{\kappa}{1+e} \frac{\dot{p}}{p}. \quad (\text{F60})$$

In the elastic domain: $\dot{\epsilon}_v = \dot{\epsilon}_v^e$. Hence, $\Delta \epsilon_v = \Delta \epsilon_v^e$ can be approximated by:

$$\Delta \epsilon_v^e = \frac{\kappa}{1+e} \Delta \ln p = \frac{\kappa}{1+e} \ln \frac{p_{n+1}}{p_n}. \quad (\text{F61})$$

F.1.2 Plastic domain

In the plastic domain, $\Delta \epsilon_v^e$ can be calculated using Equation (F61). To compute $\Delta \epsilon_v^p$, we start by taking the time derivative of yield function (5):

$$\frac{\dot{p}_c}{p_c} = \frac{\dot{p}}{p} + N \ln R \frac{q^{N-1} \dot{q}}{(Mp)^N} - N \ln R \frac{\dot{p}}{p} \left(\frac{q}{Mp} \right)^N. \quad (\text{F62})$$

Taking into account Equations (F57) and (F59), Equation (F62) can be rewritten as:

$$\frac{\dot{p}_c}{p_c} = \frac{\dot{p}}{p} \left[1 + \frac{kN \ln R}{M^N} \beta^{N-1} - \frac{N \ln R}{M^N} \beta^N \right] = \frac{\dot{\beta}}{k - \beta} + \frac{kN \ln R}{M^N} \frac{\beta^{N-1} \dot{\beta}}{k - \beta} - \frac{N \ln R}{M^N} \frac{\beta^N \dot{\beta}}{k - \beta}. \quad (\text{F63})$$

From the hardening rule (4), $\Delta \epsilon_v^p$ can be computed as:

$$\Delta \epsilon_v^p = \frac{1}{\theta} \left[-\ln(k - \beta) \Big|_{\beta_n}^{\beta_{n+1}} + \frac{kN \ln R}{M^N} \int_{\beta_n}^{\beta_{n+1}} \frac{\beta^{N-1}}{k - \beta} d\beta - \frac{N \ln R}{M^N} \int_{\beta_n}^{\beta_{n+1}} \frac{\beta^N}{k - \beta} d\beta \right]. \quad (\text{F64})$$

Denote $F_N(x)$ as the primitive integral of $\frac{x^N}{1-x}$, such that $F'_N(x) = \frac{x^N}{1-x}$, Equation (F64) can be rewritten as:

$$\Delta \varepsilon_v^p = \frac{1}{\theta} \left(-\ln(k-\beta) + \frac{k^N N \ln R}{M^N} \left[F_{N-1} \left(\frac{\beta}{k} \right) - F_N \left(\frac{\beta}{k} \right) \right] \right) \Big|_{\beta_n}^{\beta_{n+1}}. \quad (\text{F65})$$

It is noted that, in the case that N is a positive integer, $F_N(x)$ can be determined recursively as following:

$$F_0(x) = -\ln(1-x), \quad F_{N+1}(x) = F_N(x) - \frac{x^{N+1}}{N+1}. \quad (\text{F66})$$

F.2 Solution for deviatoric strain

F.2.1 Elastic domain

The rate of elastic shear strain follows by $\dot{\varepsilon}_q^e = \frac{\dot{q}}{3\mu}$, hence:

$$\dot{\varepsilon}_q^e = \frac{\kappa k}{3r(1+e)} \frac{\dot{p}}{p}. \quad (\text{F67})$$

In the elastic domain: $\dot{\varepsilon}_q = \dot{\varepsilon}_q^e$. Therefore, $\Delta \varepsilon_q = \Delta \varepsilon_q^e$ can be approximated by:

$$\Delta \varepsilon_q = \frac{\kappa k}{3r(1+e)} \Delta(\ln p) = \frac{\kappa k}{3r(1+e)} \ln \frac{p_{n+1}}{p_n}. \quad (\text{F68})$$

F.2.2 Plastic domain

In the plastic domain, $\Delta \varepsilon_q^e$ can be calculated using Equation (F68). To compute $\Delta \varepsilon_0^p$, we start first by the assumption:

$$\dot{\varepsilon}_q^p \frac{\partial g}{\partial p} = \dot{\varepsilon}_v^p \frac{\partial g}{\partial q} \Leftrightarrow \dot{\varepsilon}_q^p = \dot{\varepsilon}_v^p \frac{3(3+M) - 2M\beta}{9(M-\beta)}. \quad (\text{F69})$$

From Equations (F63) and (F69), we come up with the equation for $\dot{\varepsilon}_q^p$ which only depends on β and $\dot{\beta}$:

$$\dot{\varepsilon}_q^p = \frac{1}{\theta} \frac{3(3+M) - 2M\beta}{9(M-\beta)} \left(\frac{\dot{\beta}}{k-\beta} + \frac{kN \ln R}{M^N} \frac{\beta^{N-1} \dot{\beta}}{k-\beta} - \frac{N \ln R}{M^N} \frac{\beta^N \dot{\beta}}{k-\beta} \right). \quad (\text{F70})$$

Using the relation:

$$\frac{3(3+M) - 2M\beta}{(M-\beta)(k-\beta)} = \frac{A}{M-\beta} + \frac{B}{k-\beta}, \quad A = \frac{2M^2 - 3(3+M)}{M-k}, \quad B = \frac{3(3+M) - 2kM}{M-k}. \quad (\text{F71})$$

Then the Equation (F70) can be expanded as:

$$\begin{aligned} \dot{\varepsilon}_q^p &= \frac{A}{9\theta} \left(\frac{\dot{\beta}}{M-\beta} + \frac{kN \ln R}{M^N} \frac{\beta^{N-1} \dot{\beta}}{M-\beta} - \frac{N \ln R}{M^N} \frac{\beta^N \dot{\beta}}{M-\beta} \right) + \frac{B}{9\theta} \left(\frac{\dot{\beta}}{k-\beta} + \frac{kN \ln R}{M^N} \frac{\beta^{N-1} \dot{\beta}}{k-\beta} - \frac{N \ln R}{M^N} \frac{\beta^N \dot{\beta}}{k-\beta} \right) \\ &= \frac{A}{9\theta} \left(\frac{\dot{\beta}}{M-\beta} + \frac{kN \ln R}{M^N} \frac{\beta^{N-1} \dot{\beta}}{M-\beta} - \frac{N \ln R}{M^N} \frac{\beta^N \dot{\beta}}{M-\beta} \right) + \frac{B}{9} \dot{\varepsilon}_v^p. \end{aligned} \quad (\text{F72})$$

Which leads to the equation of $\Delta \varepsilon_q^p$:

$$\Delta \varepsilon_q^p = \frac{A}{9\theta} \left(-\ln(M-\beta) + N \ln R \left[\frac{k}{M} F_{N-1} \left(\frac{\beta}{M} \right) - F_N \left(\frac{\beta}{M} \right) \right] \right) \Big|_{\beta_n}^{\beta_{n+1}} + \frac{B}{9} \Delta \varepsilon_v^p. \quad (\text{F73})$$